Evaluation of Fluorinated m-Tyrosine Analogs as PET Imaging Agents of Dopamine Nerve Terminals: Comparison with 6-Fluorodopa

Onofre T. DeJesus, Christopher J. Endres, Steven E. Shelton, R. Jerome Nickles and James E. Holden
Department of Medical Physics and Department of Psychiatry, University of Wisconsin Medical School, Madison, Wisconsin

Fluorinated m-tyrosine analogs were evaluated as PET imaging agents and compared with 6-fluoroDOPA in the visualization of dopamine nerve terminals. **Methods:** The three m-tyrosine analogs, 6-[^{18}F]fluoro-L-m-tyrosine (6-FMT), 2-[^{18}F]fluoro-L-m-tyrosine (2-FMT) and 6-[^{18}F]fluoro-fluoromethylene-DL-m-tyrosine (6-F-FMMT), were prepared via electrophilic radiofluorination using [^{18}F]acetylhypofluorite. These three analogs, as well as 6-[^{18}F]fluoro-L-DOPA (6-FD), were injected into sets of rhesus monkeys, and serial PET images were acquired. Plasma samples were collected at different times after tracer administration, and metabolite analyses were done using high-performance liquid chromatography (HPLC). **Results:** Visual inspection of the PET images obtained using these four tracers showed that the best image contrast was obtained with 6-FMT. Patlak analysis with a reference tissue input function yielded a mean uptake rate constant for 6-FMT of 0.019 min^{-1}, a value twice those for the other tracers including 6-FD. **Conclusion:** These results demonstrate the superiority of 6-[^{18}F]FMT in visualizing dopamine terminals in the rhesus monkey brain and suggest that 6-[^{18}F]FMT is the tracer of choice in the assessment of dopamine metabolism in the living human brain.

Key Words: fluoro-m-tyrosine; 6-fluoro-L-DOPA; positron emission tomography; dopamine neurons

J Nucl Med 1997; 38:630–636

Since the first human studies visualizing dopamine terminals were reported by Garnett et al. (*1*), PET using 6-[^{18}F]fluoro-DOPA (6-FD) has become the imaging tool of choice in the study of the dopamine synthetic pathway. The analog 6-FD PET has been used to study presymptomatic parkinsonism (*2*), environmental toxin related parkinsonism (*3*) as well as in the monitoring of the survival of fetal dopamine cells implanted in parkinsonian patients (*4*). Despite these useful applications, 6-FD is not the optimal tracer to image dopamine turnover. The ubiquitous enzyme catechol-O-methyltransferase (COMT) rapidly metabolizes 6-fluoroDOPA by forming 3-O-methyl-6-fluoroDOPA (3-O-Me-6-FD). This metabolite crosses the blood-brain barrier bidirectionally and significantly contributes to background noise. Plasma metabolite analysis thus is required to correct the blood input function to properly interpret the PET data (*5*). Various pharmacological schemes to blunt the undesirable effect of 3-O-Me-6-FD have been proposed. One approach proposes the use of peripheral COMT inhibitors such as Ro 40-7592 (*6*). Another proposes to block the entry of 3-O-Me-6-FD into brain after 6-FD has penetrated the brain by administering high doses of phenylalanine to saturate the large neutral amino acid transporter (*7*). Although the desired improvement associated with reduced brain entry of 3-O-Me-6-FD was observed with either pharmacological intervention, systemic effects of these treatments may limit their use in routine human studies.

We have previously proposed a chemical approach to circumvent the metabolite problem associated with 6-FD (*8*). This approach examined the possible use of noncatecholic DOPA analogs that, unlike L-DOPA, are not COMT substrates since they lack the catechol structure. Since decarboxylation is critical to the retention of 6-FD in the monkey brain (*9*), useful noncatechols also must be substrates of L-aromatic amino acid decarboxylase (LAAAD, EC 4.1.1.28). One of the family of compounds we proposed for this purpose was m-tyrosine (*8*). Meta-tyrosine is a DOPA analog found to offer protection against dopamine depletion induced by reserpine treatment in rodents, suggesting its possible use in the therapy of Parkinson's disease (*10*). However, subsequent clinical trials failed to show the utility of m-tyrosine in the treatment of parkinsonian patients (*11*).

Comparison of the major metabolic pathways for L-DOPA and L-m-tyrosine (Fig. 1) demonstrates the significant simplification of the metabolism of L-m-tyrosine relative to L-DOPA. Also depicted in Figure 1 is the metabolism of a novel analog of m-tyrosine, (E)-β-fluoro-methylene-L-m-tyrosine (FMMT) that is transformed by LAAAD to an amine that binds monoamine oxidase (MAO) irreversibly (*12*). Because of this possible trapping mechanism, L-FMMT has the potential of being the tracer of choice for assessing LAAAD activity (*13*). In this study, in order to test the hypothesis that simplification of metabolism would lead to improved tracer properties, we have performed PET studies using normal rhesus monkeys to compare the ability of 6-fluoro-m-tyrosine (6-FMT), 2-fluoro-m-tyrosine (2-FMT), 6-fluoro-fluoro-methylene-m-tyrosine (6-FFMMT) and 6-fluoroDOPA (6-FD) to image dopamine nerve terminals.

Previous reports on work involving monkeys (*14*) and humans (*15*) have confirmed our expectation that fluoro-m-tyrosine (FMT) analogs will provide better PET image contrast compared to 6-FD. Interestingly, both studies found that at later time points after administration, the major ^{18}F metabolite of FMT in both blood and brain in rats and monkeys was fluoro-m-hydroxy-phenylacetic acid (FHPAA) that presumably is formed by the successive decarboxylation of FMT to fluoro-m-tyramine (FMTA) followed by oxidation to FHPAA by monoamine oxidase (MAO). In this study, in conjunction with PET imaging, we also performed plasma metabolite analysis in each PET study to establish the contributions of the respective labeled metabolites of each tracer to the PET data.

MATERIALS AND METHODS

Synthesis of Tracers and Metabolites

The analog 6-[^{18}F]fluoro-L-DOPA (6-FD) was prepared using the method of Adam and Jivan (*16*). The starting material used, a

Received Mar. 19, 1996; revision accepted Jul.15, 1996.
For correspondence or reprints contact: Onofre T. DeJesus, MD, Dept. of Medical Physics, University of Wisconsin Medical School, 1530 Medical Sciences Center, 1300 University Ave., Madison, WI 53706.

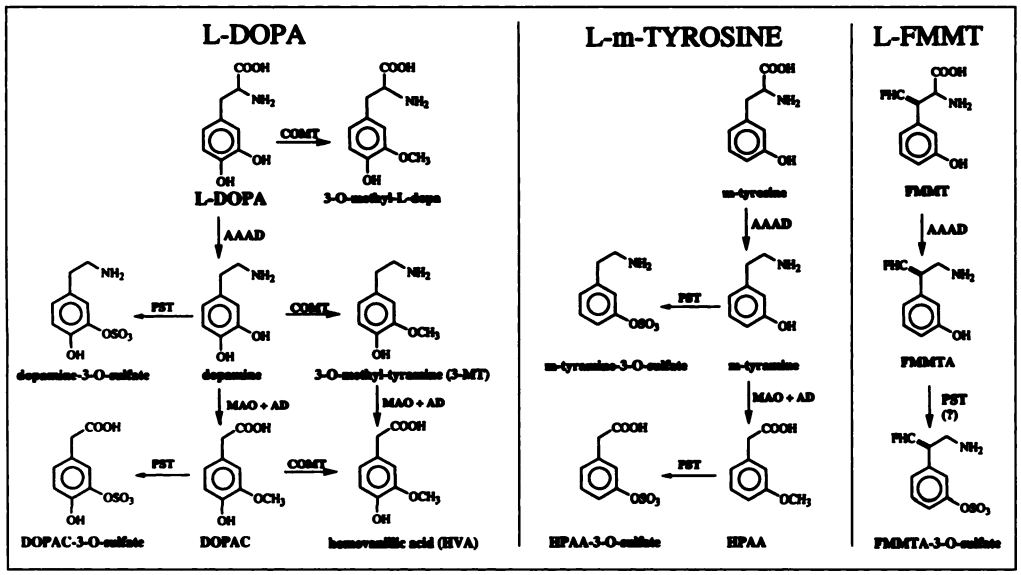

FIGURE 1. Simplified metabolism of L-DOPA, L-m-tyrosine and (E)β-fluoromethylene-L-m-tyrosine (L-FMMT) showing the major pathways. The enzymes involved are L-aromatic amino acid decarboxylase (AAAD), catechol-O-methyltransferase (COMT), monoamine oxidase (MAO), adenine dehydrogenase (AD) and phenolsulfotransferase (PST).

mercurated and protected L-DOPA derivative, was purchased from BOZ Chem. Engr. (Quebec, Canada). 6-FD metabolites, 6-fluorodopamine, 3-O-Me-6-FD, 6-FDOPAC, 6-FHVA and 3-O-Me-6-fluoro-p-tyramine, were prepared by the direct fluorination of the parent compounds with acetylhypofluorite followed by HPLC isolation and ^{1}H and ^{19}F NMR characterization (*17*).

The analogs 6-[^{18}F]fluoro- and 2-[^{18}F]fluoro-m-tyrosine were prepared as previously reported (*18*). Authentic samples of the metabolites, 6-fluoro- and 2-fluoro-m-hydroxyphenylacetic acid, were prepared from m-methoxyphenylacetic acid and acetylhypofluorite while 6-fluoro- and 2-fluoro-m-tyramine were prepared from m-methoxyphenylalanine. After demethylation with HI and HPLC purification, ^{1}H and ^{19}F NMR characterization were done to confirm the identity of the compounds. NMR results were consistent with those reported by Chirakal et al. (*19*) for the same compounds and identified these compounds as the desired metabolites.

The 6-[^{18}F]fluoro-(E)-β-fluoromethylene-DL-m-tyrosine (6-FFMMT) was prepared as previously reported (*20*). Direct fluorination of the decarboxylated FMMT, (E)-β-fluoromethylene-m-tyramine (FMMTA), which was provided by Merrell Dow Research Institute (Cincinnati, OH), gave a product whose HPLC retention time was consistent with a labeled metabolite formed when 6-[^{18}F]F-FMMT was incubated with rat liver homogenate (DeJesus et al., unpublished). The chemically synthesized product was tentatively identified as a mixture of ring-fluorinated isomers of FMMTA. Recently, in support of this identification, Schoun et al. (*21*) found, by extensive gas chromatography/mass spectrometry (GC/MS) studies of plasma after administration of deuterated FMMT in human volunteers, that the main plasma metabolite of FMMT is indeed the decarboxylated amine, FMMTA.

High-Performance Liquid Chromatography

For plasma and tissue analysis for labeled metabolites, a sensitive HPLC flowthrough βγγ triple coincidence detector (*22*) was used. The HPLC system consisted of an Alltech Econosphere C-18 column 3μ (100 × 4.6 mm) and the ion-pairing mobile phase used consisted of octyl sulfonate, chloroacetic acid, n-butylamine, EDTA, pH 3.5 and 0%–10% methanol.

PET Studies

The adult rhesus macaques used in this study were drawn from the colony housed in the Wisconsin Regional Primate Center (WPRC). The animals were fasted overnight and pretreated with carbidopa (2 mg/kg, nasogastric) 1 hr before the study. On the day of the study, the animal was anesthetized initially with ketamine hydrochloride (15 mg/kg IM) to allow the placement of arterial (posterior tibial artery) and venous angiocath lines and transport of the animal from WRPC to the UW PET facility. In the PET facility the animal was positioned in a Siemens CTI 933/04 PET scanner which acquires seven image planes simultaneously with an interplanar distance of 6.75 mm. Anesthesia was maintained for the duration of the PET study with 1%–2% isoflurane. A transmission scan was performed to confirm positioning and for later correction of the emission data for attenuation. Radiotracer was administered as an intravenous bolus. The dynamic image scan sequence, initiated simultaneously with the tracer bolus injection, consisted of five 2-min frames and at least eight 10-min frames. A small number of arterial blood samples was collected from the arterial angiocath line during the PET studies. Total blood drawn in a day was held to a maximum of 20 ml/animal. After the dynamic image sequence, an emission scan was acquired. A 15-min acquisition was performed in the same axial position used in the dynamic study. This was followed immediately by a second 15-min acquisition with axial position offset by half an interplane distance, providing a final axial sampling interval of 3.375 mm.

To compare pharmacokinetics and image quality obtainable from each tracer, [^{18}F]2-FMT, [^{18}F]6-FMT and [^{18}F]6-FFMMT as well as [^{18}F]6-fluoroDOPA were studied. A total of 13 studies was performed on eight monkeys with the four tracers. Table 1 describes the subjects used in these studies and the tracer dose given. The 6-FFMMT studies involved female monkeys, one of which was studied twice, while the rest of the studies with the other tracers involved male monkeys. Gender is not known to be a confounding factor in these studies.

Plasma Metabolite Analyses

Blood samples collected from the animal during the study were transferred to Eppendorf vials containing 1% Na_2EDTA solution and kept in ice. Plasma, separated from whole blood by centrifugation at 1000 g at 4°C, was deproteinized with 4 *M* $HClO_4$ with 0.1% NaS_2O_3 and 7.5% Na_2EDTA and centrifuged at 17000 g at 4°C. Supernatant fractions were directly analyzed by radio HPLC. Extraction efficiencies for this procedure for 6-FD are reported to be about 94% (*23*). Extraction efficiency for 6-fluoro-m-tyrosine was found to be quantitative, thus the values obtained in the assay of metabolites were used uncorrected.

Image Data Analysis

The interleaved dataset was used to select the plane in the dynamic study that contained the maximal signal in the striatal region. ROIs were then placed in this plane to cover both left and

TABLE 1
Summary Description of Monkey Subjects and Tracer Dose Injected in PET Studies

Subject no.	Sex	Age (yr)	Weight (kg)	Tracer dose (mCi)			
				6-FD	6-FMT	2-FMT	6-FFMMT
1142	F	>30	5.8	—	—	—	1.5
78087	F	13	6.1	—	—	—	1.5, 1.9
86005	M	6	6.2	3.4	—	—	—
78093	M	13	10.1	2.9	—	—	—
85081	M	6	9.1	3.4	—	—	—
83121	M	9	11.5	2.8	5.8	2.9	—
85007	M	8	9.0	3.4	4.3	3.4	—
81153	M	11	9.1	—	4.6	—	—

right striatum (usually dominated by the putamen) and occipital cortex. Time courses of radioactivity concentration averages were then generated for each region. These were standardized in each study by dividing the mean concentration values in each region (microCi/g brain) by the mean whole-body concentration (injected dose (mCi)/whole-body mass (g)). This dimensionless concentration ratio was then multiplied by 100 to yield percent relative concentration. For the 6[^{18}F]F-DL-FMMT studies, the standardization was performed using half the injected dose since the D isomer was previously found not to be transported into the brain (*13*). The standardized time courses (percent relative concentration) were then averaged at each time point to provide representative average time courses for each tracer.

Unstandardized time courses from each individual study were used to estimate uptake rates by the graphical method (*24*) with the time course in occipital cortex used as an input function for the striatal uptake (*25*). Only data beyond 30 min after injection were used for the linear fit.

RESULTS

PET Studies

Figure 2 shows PET images obtained using each of the four tracers for three overlapping transverse brain slices (6.75 mm thick/slice and 3.375 mm apart) stepping inferiorly from left to right with the rightmost slice being the most caudal. The outer rim of the images (Fig. 2), which show high extracerebral (muscles) tracer localization, is most prominent in the 2-FMT and 6-FD images compared to 6-FMT images. This tracer localization in muscles as well as in some extrastriatal areas may indicate nonspecific localization and/or localization of metabolite. In the case of 6-FD, the PET signal in muscle is probably [^{18}F]3-O-Me-6-FD since parent 3-O-Me-DOPA is known to penetrate and slowly leave muscle tissue (*26*).

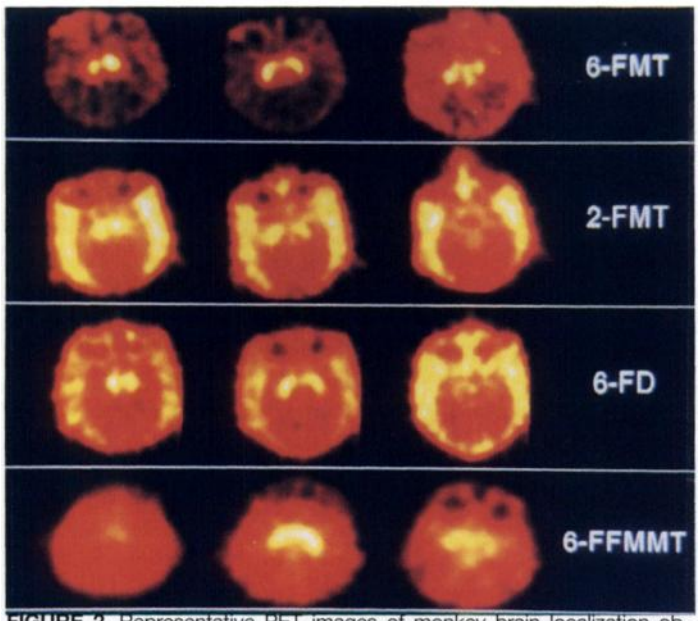

FIGURE 2. Representative PET images of monkey brain localization obtained with the tracers 6-[^{18}F]fluoro-m-tyrosine (6-FMT), 2-[^{18}F]fluoro-m-tyrosine (2-FMT), 6-[^{18}F]fluoro-L-DOPA (6-FD) and 6-[^{18}F]fluoro-(E)-β-fluoromethylene-DL-m-tyrosine (6-FFMMT). A hot metal scale is used; black to red to yellow to white represent increasing radioactivity. See text for more detailed description.

Time-Activity Curves

A comparison of the mean time courses of the four tracers is plotted in Figure 3. Since the occipital cortex is poorly innervated with dopamine terminals, the ratio of striatal (str) to cortical (ctx) uptake can be taken as a measure of image contrast which represents specific to nonspecific localization. The time course of str/ctx ratio for each tracer is shown in Figure 4. While the str/ctx ratio for 6-FMT 85 min after tracer injection is 5.8, the values for 2-FMT, 6-FFMMT and 6-FD were in the 2.1–2.8 range. Uptake rate values for the four tracers calculated by the graphical method with the cortical time course as input function are summarized in Table 2. The mean Ki found for 6-FMT is more than twice that for 6-FD while 2-FMT has a Ki value 20% lower than that for 6-FD.

HPLC Metabolite Analyses

Typical HPLC chromatograms of plasma analysis of samples collected 30 min after tracer injection of each of the four tracers, 6-FD, 6-FMT, 2-FMT and 6-FFMMT, are shown in Figure 5. Samples obtained at other times after injection were similarly analyzed. The amount of each labeled species was then expressed as a percent of the total radioactivity in each sample and thus measures relative, rather than absolute, concentrations. The time course of the relative amounts of the observed plasma metabolites for each of these four tracers are plotted in Figure 6. The 6-fluoroDOPA was found to have several metabolites in monkey blood while each of the three m-tyrosine derivatives were found to have two metabolites. The 6-fluoroDOPA (retention time, t_r = 5 min) and its main metabolites, 3-O-Me-6-FD (t_r = 13.5 min) and 6-FHVA (t_r = 36 min), were identified using authentic standards (*17*). Several unidentified peaks in the chromatograms are probably the conjugates of 6-FDA and 6-FDOPAC (*27,23*).

The late-eluting plasma metabolites of 6-FMT and 2-FMT were identified, by comparison with authentic samples, as the corresponding fluoro-m-hydroxyphenylacetic acids (6- and 2-FHPAA) (t_r = 10 min and 11 min, respectively) while the metabolites found to be more polar than FMT are probably sulfoconjugates (t_r = 2.5 min and 2 min for 6- and 2-fluoro isomers, respectively) as suggested by others (*14,15*). The plasma metabolites of 6-F-FMMT (t_r = 3.8 min) were identified as 6-fluoro-fluoromethylene-m-tyramine (6-F-FMMTA)

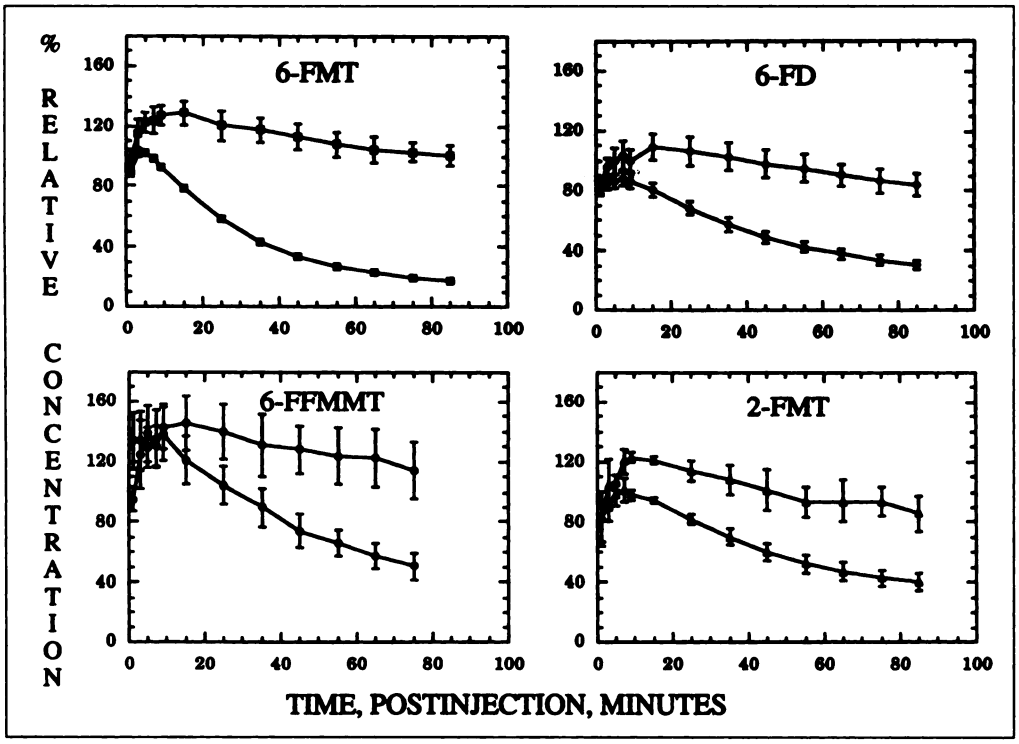

FIGURE 3. Multiple time-activity plots for two brain regions, striatum (upper curve) and occipital cortex (lower curve), for 6 FMT (squares), 6-FD (diamonds), 6-FFMMT (circles) and 2-FMT (triangles). The label on the vertical axis arises from dividing radioactivity concentrations (microCi/g) by the mean whole-body concentration (injected dose/whole-body mass) and multiplying by 100 to give percent relative concentration. Error bars for each point in these standardized time courses are the s.e.m. of two to five studies for each tracer (Table 1).

(t_r = 13.5 min), and the other more polar metabolite (t_r = 2 min) is probably also a sulfoconjugate similar to that suggested for FMT.

DISCUSSION

In addition to 6-Fluoro-L-DOPA, several PET tracers have recently been suggested to image dopamine nerve terminals. These proposed new tracers bind dopamine transporter molecules either at the neuronal membrane such as the cocaine analog WIN 35148 (*28*) and methylphenidate (*29*) or at the storage vesicular membrane such as a tracer based on the compound tetrabenazine (*30*). At the present time, however, only 6-FD uptake values have been shown to directly correlate with dopamine cell number counted postmortem both in MPTP lesioned monkeys (*31*) and in Parkinson's disease patients (*32*). Although approaches using transporter molecules to assess dopamine neurodegeneration associated with Parkinson's disease have been shown to be useful, PET imaging using 6-FD and its analogs, which assess a metabolic step in dopamine synthesis related to neuronal activity rather than number of neurons, provide more physiological information about the functional status of dopamine neurons. Although transporter molecules may prove to be the tracers of choice to measure surviving dopamine neurons in neurodegenerative diseases, assessing changes in rates of biochemical reactions in the intact dopaminergic system accompanying neuro-psychiatric disorders and addictive and violent behaviors will require metabolic tracers such as those described in this study.

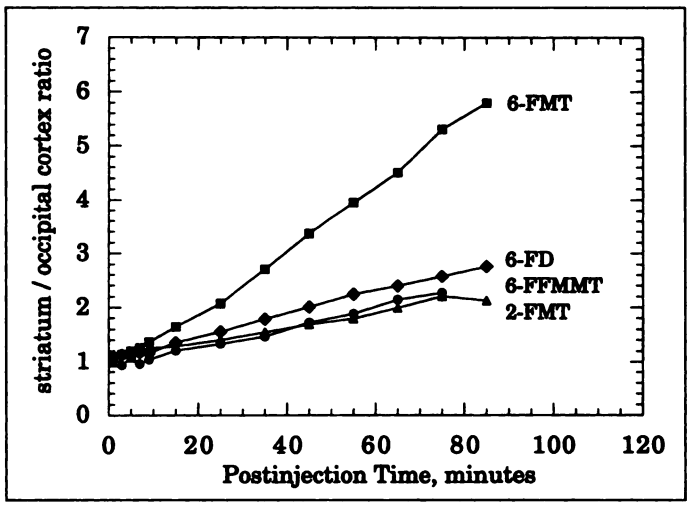

FIGURE 4. Time course of striatum to occipital cortex (str/ctx) ratio obtained from the multiple time-activity plots (Fig. 3) for the four tracers.

By comparing the images shown in Figure 2, it is clear that 6-FMT gives images with the highest contrast (specific-to-nonspecific uptake). With such image contrast, it is likely that PET with 6-FMT can allow visualization of nonstriatal dopamine in such small areas as the substantia nigra. The central hot spot observed in the rightmost 6-FMT image (Fig. 2) demonstrates such uptake in nonstriatal areas. Identification of these areas is currently being investigated by correlating PET images obtained using the new GE Advance PET scanner at the UW PET Clinic with MR images of these animals' brains. Planned human studies also are expected to clarify these extrastriatal localizations.

The high image contrast obtained with 6-FMT most probably is due to the absence of metabolites produced by peripheral COMT and, as suggested by Firnau et al. (*15*), the faster and more efficient clearance of the unretained 6-FMT from nondopaminergic regions such as occipital cortex (Fig. 3). Although 6-F-FMMT, which requires conversion to 6-F-FMMTA to be retained in the striatum (*13*), has the possible advantage of

TABLE 2
Mean Uptake Constants for 6-FMT, 6-FD, 6-FFMMT and 2-FMT in Monkey Brain

Tracer	Mean Ki, $min.^{-1}$ ± s.d.	Number of studies
6-FMT	0.0187 ± 0.0005	3
6-FD	0.0089 ± 0.0005	5
6-FFMMT	0.0092 ± 0.0008	3
2-FMT	0.0069 ± 0.0009	2

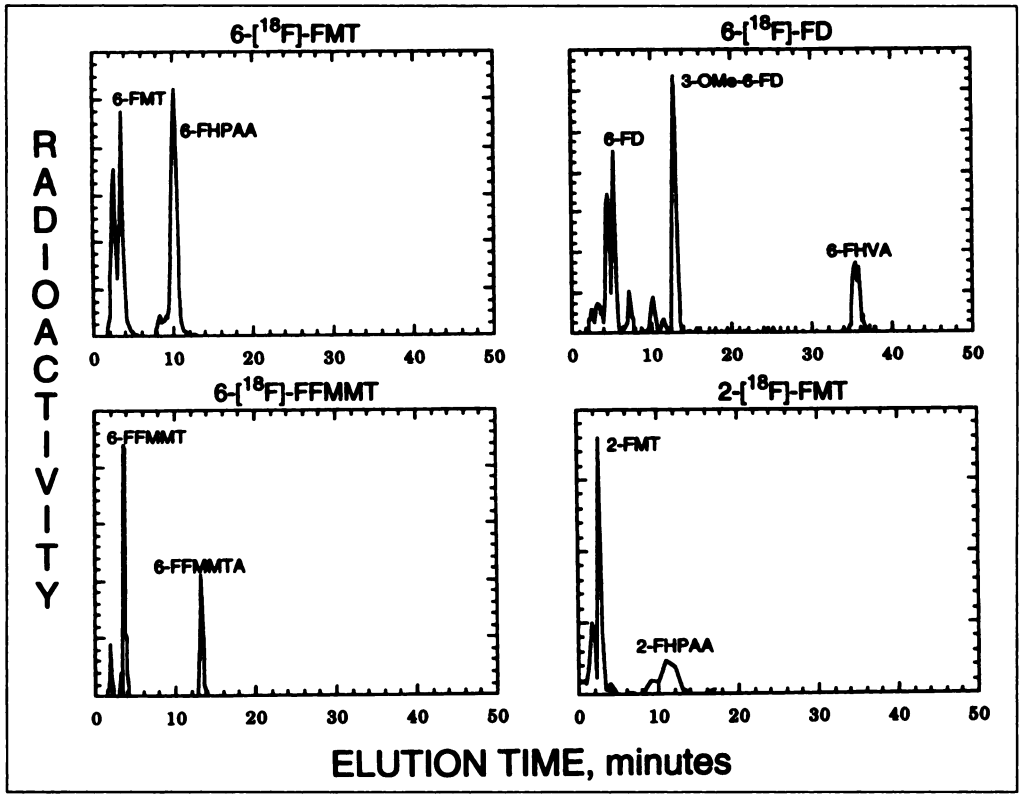

FIGURE 5. Representative radiochromatograms obtained in the analyses of plasma taken from a monkey 30 min after the injection of each of the four tracers. In each case, a labeled conjugate is seen to elute before the unchanged tracer.

irreversibly binding MAO in dopamine terminals, the clearance of this tracer from the occipital cortex is not as extensive as the clearance of 6-FMT from this nondopaminergic region. The high contrast of 6-FMT images is further emphasized in the plots of the time course of str/ctx ratios for each tracer shown in Figure 4 and the mean Patlak uptake constants listed in Table 2. The Ki values confirm the superiority of 6-FMT as a tracer when compared to 6-FD, 6-F-FMMT and 2-FMT. The improved uptake constant of 6-FMT is expected to also result in improved sensitivity of 6-FMT studies to changes in dopamine turnover compared to 6-FD scans.

The metabolic profile of 6-FMT in blood, shown in Figure 5, confirms the finding of Firnau et al. (*15*) that the main blood metabolite after the intravenous injection of 6-FMT is 6-fluorohydroxyphenylacetic acid (6-FHPAA). As further demonstrated by Firnau et al. (*33*), this polar peripheral metabolite does not cross the blood-brain barrier and does not contribute to the PET image in contrast to the confounding contribution of 3-O-Me-

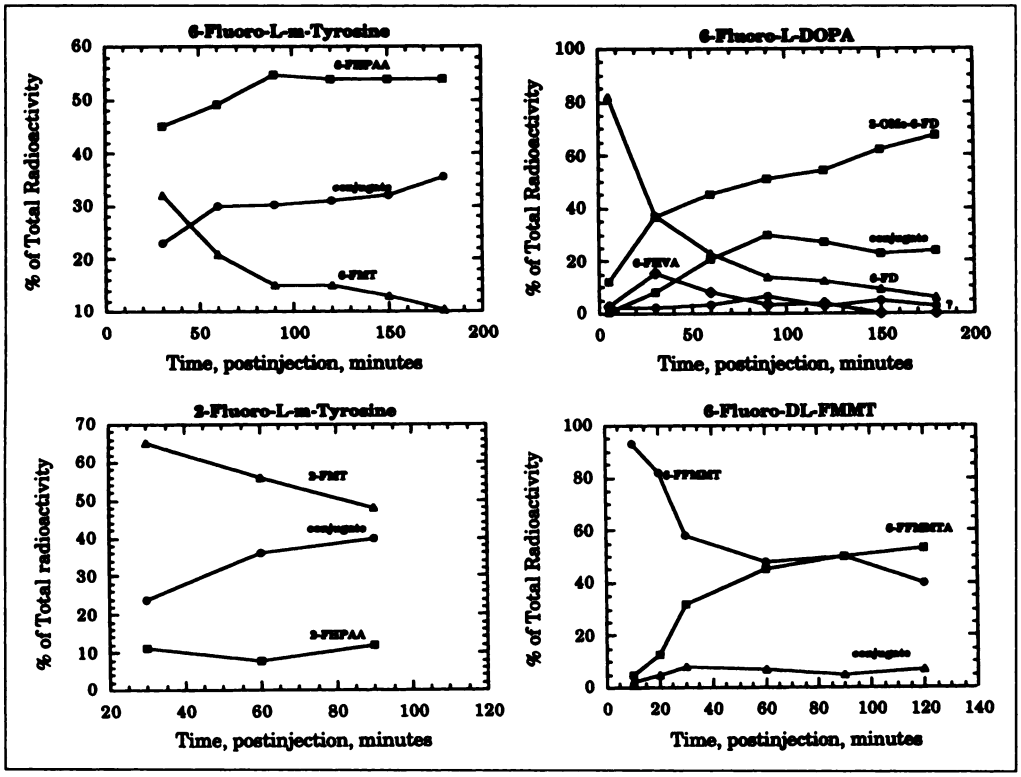

FIGURE 6. Time courses of the different metabolites formed in plasma after injection of each of the four tracers into rhesus monkeys using data obtained by radio HPLC analyses as exemplified in Figure 5.

6-FD in 6-FD studies. The metabolic profile of 2-FMT was found to be similar to that of 6-FMT. However, 2-FMT appears to be a poorer LAAAD substrate compared to 6-FMT as seen in the low levels of 2-FHPAA observed. It may also be possible that 2-FHPAA clears blood faster than 6-FHPAA perhaps due to the higher acidity of ortho-fluorophenol compared to para-fluorophenol. On the other hand, for 6-FFMMT, the putative decarboxylated product, 6-FFMMTA, may also be a suicide inhibitor of MAO like its parent FMMTA. If this is the case, 6-FFMMTA may not be further metabolized by MAO which is consistent with the finding of a metabolite identified as 6-FFMMTA. The other more polar metabolite observed is most likely a sulfoconjugate analogously to the other m-tyrosine compounds. The time course of the blood metabolism of 6-FFMMT, which was given as the racemic mixture, show that unchanged 6-FFMMT levels off between 1 hr to 2 hr to about 50% of the total plasma radioactivity. Because of the stereoselectivity of LAAAD, it is likely that the unmetabolized tracer observed is mostly the D isomer of 6-FFMMT which we previously demonstrated not to cross into the brain (*13*).

One interesting observation of Firnau et al. (*15*) was that 6-fluoro-hydroxyphenylacetic acid (6-FHPAA) is the major labeled metabolite, in vivo, of 6-FMT in rhesus monkey brain. This indicates that 6-[^{18}F]F-HPAA dominates the striatal signal in the PET images. In order to better understand this finding we have done in vivo microdialysis in rats. We have also analyzed whole striatal tissue that measures the sum of extracellular and intracellular metabolites. Knowing both total and extraneuronal metabolite profiles may be useful in understanding the role of metabolites in the PET data. Preliminary results show that the fraction of 6-FHPAA with respect to the total ^{18}F-labeled compounds observed in extracellular space is similar to the fraction of 6-FHPAA found in the whole striatum 30 min after tracer administration (DeJesus et al., unpublished data). This preliminary finding suggests that 6-FHPAA freely diffuses across neuronal membrane and that the PET images obtained in monkey brain at later times after 6-FMT injection are based on intra- and extraneuronal 6-FHPAA and its sulfoconjugate both of which appear to clear slowly from the region where they are formed. This is unlike the corresponding dopamine metabolite, DOPAC, whose formation provides the major route in the elimination of dopamine from mammalian brain. A possible explanation for the difference between the clearance of FHPAA and DOPAC may be the fact that the COMT pathway, which is used in the elimination of 70% of unwanted dopamine (*34*), is not available to FHPAA. Thus, the very slow clearance of FHPAA can result from a combination of three factors: (a) slow brain egress of FHPAA; (b) slow sulfoconjugation of FHPAA; and (c) slow brain egress of FHPAA-SO_4. Whatever the underlying mechanism of clearance for FHPAA is, the persistence of high contrast in dopamine terminals in the PET images suggests that, within the time frame of the PET study, ^{18}F radioactivity is essentially trapped.

CONCLUSION

We have evaluated three noncatecholic L-DOPA analogs as possible imaging agents for dopamine terminals. Results obtained in this study suggest that 6-FMT is superior to the currently used tracer 6-FD and is likewise better than two other FMT analogs, 2-FMT and 6-FFMMT. The superior image contrast obtained with 6-FMT appears to result from the slow brain clearance of 6-FHPAA, a metabolite formed by the successive decarboxylation and oxidation of 6-FMT, and another metabolite, most likely a sulfoconjugate. Recent PET studies have shown the utility of 6-[^{18}F]FMT in the assessment of dopamine function in MPTP-lesioned monkeys (*35*). Furthermore, recent human studies reported by Nahmias et al. (*36*) support the superiority of 6-FMT as the imaging agent for decarboxylation in dopamine terminals suggesting that 6-FMT is the PET tracer of choice to assess dopamine metabolism in the living brain.

ACKNOWLEDGMENTS

We gratefully acknowledge the financial support of NIH grants NS 26621 (OTD) and AG10217 (JEH) and the American Parkinson's Disease Association. This paper was presented at the 42nd Annual Meeting of the Society of Nuclear Medicine in Minneapolis, MN, on June 12–15, 1995.

REFERENCES

1. Garnett ES, Firnau G, Nahmias C. Dopamine visualized in the basal ganglia of living man. *Nature* 1983;305:137–138.
2. Sawle GV, Wroe SJ, Lees AJ, Brooks DJ, Frackowiak RS. The identification of presymptomatic parkinsonism: clinical and [18F]DOPA positron emission tomography studies in an Irish kindred. *Ann Neurol* 1992;32:609–617.
3. Tetrud JW, Langston JW, Irwin I, Snow BJ. Parkinsonism caused by petroleum waste ingestion. *Neurology* 1995;14:1051–1054.
4. Freed CR, Breeze RE, Rosenberg NL, et al. Survival of implanted fetal dopamine cells and neurologic improvement 12 to 46 mo after transplantation in Parkinson's disease. *J New Engl Med* 1992;327:1549–1555.
5. Dhawan V, Ishikawa T, Patlak C, et al. Combined FDOPA and 3OMFD PET studies in Parkinson's disease. *J Nucl Med* 1996;37:209–216.
6. Ruottinen HM, Rinne JO, Ruotsalainen UH, et al. Striatal[^{18}F]fluorodopa utilization after COMT inhibition with entecapone studied with PET in advanced Parkinson's disease. *J Neural Transm [P-D Sect]* 1995:10:91-106.
7. Doudet DJ, McLellan CA, Aigner TG, et al. Postinjection L-phenylalanine increases basal ganglia contrast in PET scans of 6-^{18}F-DOPA. *J Nucl Med* 1991;32:1408–1413.
8. DeJesus OT, Mukherjee J. Radiobrominated m-tyrosine analog as a potential CNS L-DOPA PET tracer. *Biochem Biophys Res Commun* 1988;150:1027–1031.
9. Pate BD, Snow BJ, Hewitt KA, Morrison KS, Ruth TJ, Calne DB. The reproducibility of striatal uptake obtained with positron emission tomography and fluorine-18-L-6-fluoroDOPA tracer in nonhuman primates. *J Nucl Med* 1991;32:1246–1251.
10. Carlsson A, Lindquist M. Metatyrosine as a tool for selective protection of catecholamine stores against reserpine. *Eur J Pharmacol* 1967;2:187–192.
11. Cotzias GC, Papavasiliou PS, Mena I. L-m-tyrosine and parkinsonism. *JAMA* 1973;223:83.
12. Palfreyman MJ, McDonald IA, Fozard JR, et al. Inhibition of monoamine oxidase selectively in brain monoamine nerves using the bioprecursor (E)β-fluoromethylene-m-tyrosine (MDL 72394), a substrate for aromatic L-amino acid decarboxylase. *J Neurochem* 1985;45:1850–1860.
13. DeJesus OT, Holden JE, Endres C, et al. Visualization of dopamine nerve terminals by positron emission tomography using [^{18}F]fluoro-β-fluoromethylene-m-tyrosine. *Brain Res* 1992;597:151–154.
14. Melega WP, Perlmutter MM, Luxen A, et al. 4-[^{18}F]fluoro-m-tyrosine: an L-3,4-dihydroxyphenylalanine analog for probing presynaptic dopaminergic function with positron emission tomography. *J Neurochem* 1989;53:311–313.
15. Firnau G, Chirakal R, Nahmias C, Garnett ES. [^{18}F]fluoro-meta-tyrosine is a better PET tracer than [F18]fluoro-L-Dopa for the delineation of dopaminergic structures in the human brain. *J Label Comp Radiopharm* 1991;30:266–268.
16. Adam MJ, Jivan S. Synthesis and purification of L-6[^{18}F]fluorodopa. *Appl Radiat Isot* 1988;39:1203–1206.
17. Nickles RJ, DeJesus OT. Frugal PET: is it possible? In: Emran AM, ed. *Chemists' views of imaging centers*. New York: Plenum Press; 1995:133–139.
18. DeJesus OT, Sunderland JJ, Nickles RJ, Mukherjee J, Appelman EV. Synthesis of radiofluorinated analogs of m-tyrosine as potential L-Dopa tracers via direct reactions with acetylhypofluorite. *Appl Radiat Isot* 1990;41:433–437.
19. Chirakal R, Schrobilgen GJ, Firnau G, Garnett ES. Synthesis of [^{18}F]-labeled fluoro-m-tyrosine, fluoro-m-tyramine and fluoro-m-hydroxyphenylacetic acid. *Appl Radiat Isot* 1991;42:113–117.
20. Murali D, DeJesus OT, Sunderland JJ, Nickles RJ. [^{18}F]-β-fluoro-methylene-m-tyrosine, a potential PET agent for presynaptic dopamine terminals: synthesis and spectroscopic characterization. *Appl Radiat Isot* 1995;43:969–977.
21. Schoun J, Dulery B, Haegele KD. Validation of a gas chromatographic/mass spectrometric method for the determination of (E)β-fluoro-methylene-m-tyrosine and its active metabolite in human plasma and urine. *Biol Mas Spect* 1992;21:625–632.
22. Nickles RJ, DeJesus OT, Solin OH, Harparaanta M. A flow-through detector for nanocurie activities encountered in HPLC analysis of PET tracer metabolites. *IEEE Trans Nucl Sci* 1992;39:2316–2321.
23. Chan GL-Y, Hewitt KA, Pate BD, Schofield P, Adam MJ, Ruth TJ. Routine determination of [^{18}F]-L-6-fluorodopa and its metabolites in blood plasma is essential for accurate positron emission tomography studies. *Life Sci* 1992;50:309–318.
24. Patlak CS, Blasberg RG. Graphical evaluation of blood-to-brain transfer constants from multiple-time uptake data. *Generalizations J Cereb Blood Flow Metab* 1985;5:584–590.
25. Brooks DJ, Ibanez V, Sawle GV, et al. Differing patterns of striatal ^{18}F-Dopa uptake in Parkinson's disease, multiple system atrophy and progressive supranuclear palsy. *Ann Neurol* 1990;28:547–555.
26. Deleu D, Sarre S, Ebinger G, Michotte Y. In vivo pharmacokinetics of levodopa and

3-O-methyldopa in muscle. A microdialysis study. *Naunyn Schmiedeberg Arch Pharmacol* 1991;34:514–519.
27. Claustre J, Pequignot JM, Bui-xian B, Muchada R, Cottet-Emard RM, Peyrin L. Conjugation and deamination of circulating dopamine: relationship between sulfated and free dopamine in man. *J Auton Nerv Sys* 1990;29:175–182.
28. Frost JJ, Rosier AJ, Reich SG, et al. Positron emission tomographic imaging of the dopamine transporter with 11C-WIN 35428 reveals marked declines in mild Parkinson's disease. *Ann Neurol* 1993;34:423–431.
29. Volkow N, Ding YS, Fowler JS, et al. A new PET ligand for the dopamine transporter: studies in the human brain. *J Nucl Med* 1995;36:2252–2260.
30. VanderBorght TM, Kilbourn MR, Koeppe RA, et al. In vivo imaging of the brain vesicular monoamine transporter. *J Nucl Med* 1995;36:2162–2168.
31. Pate BD, Kawamata T, Yamada T, et al. Correlation of striatal fluoroDOPA uptake in the MPTP monkey with dopaminergic indices. *Ann Neurol* 1993;34:331–338.
32. Snow BJ, Tooyama I, McGeer EG, et al. Human positron emission tomographic [^{18}F]fluoroDOPA studies correlate with dopamine cell counts and levels. *Ann Neurol* 1993;34:324–330.
33. Firnau G, Chirakal R, Nahmias C, Garnett ES. Do the metabolites of [F18]fluoro-L-Dopa and [^{18}F]fluoro-meta-tyrosine contribute to the accumulation of [F-18] in the human brain? *J Label Comp Radiopharm* 1991;30:293–294.
34. Dedek J, Baumes R, Tien-Duc N, Gomeni R, Korf J. Turnover of free and conjugated (sulphonyloxy)dihydroxyphenylacetic acid and homovanillic acid in rat striatum. *J Neurochem* 1979;33:687–695.
35. O'Neil JP, VanBrocklin HF. Development of a semi-remote system for the routine preparation of [^{18}F]6-fluoro-L-meta-tyrosine to study striatal lesions and therapeutic implants in primates [Abstract]. *J Labelled Comp Radiopharm* 1995;37:655–657.
36. Nahmias C, Wahl L, Chirakal R, Firnau G, Garnett ES. A probe for intracerebral aromatic amino acid decarboxylase activity: distribution and kinetics of [^{18}F]6-fluoro-L-m-tyrosine in the human brain. *Movement Disorders* 1995;10:298–304.

Three-Dimensional Imaging Characteristics of the HEAD PENN-PET Scanner

Joel S. Karp, Richard Freifelder, Michael J. Geagan, Gerd Muehllehner, Paul E. Kinahan, Robert M. Lewitt and Lingxiong Shao

Department of Radiology, University of Pennsylvania; UGM Medical Systems, Philadelphia, Pennsylvania

A volume-imaging PET scanner, without interplane septa, for brain imaging has been designed and built to achieve high performance, specifically in spatial resolution and sensitivity. The scanner is unique in its use of a single annular crystal of NaI(Tl), which allows a field of view (FOV) of 25.6 cm in both the transverse and axial directions. Data are reconstructed into an image matrix of 128^3 with $(2\ mm)^3$ voxels, using three-dimensional image reconstruction algorithms. **Methods:** Point-source measurements are performed to determine spatial resolution over the scanner FOV, and cylindrical phantom distributions are used to determine the sensitivity, scatter fraction and counting rate performance of the system. A three-dimensional brain phantom and ^{18}F-FDG patient studies are used to evaluate image quality with three-dimensional reconstruction algorithms. **Results:** The system spatial resolution is measured to be 3.5 mm in both the transverse and axial directions, in the center of the FOV. The true sensitivity, using the standard NEMA phantom (6 liter), is 660 kcps/μCi/ml, after subtracting a scatter fraction of 34%. Due to deadtime effects, we measure a peak true counting rate, after scatter and randoms subtraction, of 100 kcps at 0.7 mCi for a smaller brain-sized (1.1 liter) phantom, and 70 kcps for a head-sized (2.5 liter) phantom at the same activity. A typical ^{18}F-FDG clinical brain study requires only 2 mCi to achieve high statistics (100 million true events) with a scan time of 30 min. **Conclusion:** The HEAD PENN-PET scanner is based on a cost-effective design using NaI(Tl) and has been shown to achieve high performance for brain studies and pediatric whole-body studies. As a full-time three-dimensional imaging scanner with a very large axial acceptance angle, high sensitivity is achieved. The system becomes counting-rate limited as the activity is increased, but we achieve high image quality with a small injected dose. This is a significant advantage for clinical imaging, particularly for pediatric patients.

Key Words: three-dimensional volume imaging; positron emission tomography scanner performance

J Nucl Med 1997; 38:636–643

PET is an imaging modality that has made major advances in recent years. The spatial resolution is improved through better detector design, and the sensitivity is improved with three-dimensional imaging and through an increase in the axial field of view. These improvements, however, have generally been accompanied by an increase in cost of the instrument. While the interest in PET continues to grow and the applications broaden, it is important that the cost of the technology does not outpace its clinical utility. Our major objectives in designing a new PET scanner were to achieve high isotropic spatial resolution and sensitivity for clinical brain studies in a cost-effective design. Design criteria were chosen to optimize these measures of performance, while tradeoffs in other areas were made.

Three basic choices were made in the design of the HEAD PENN-PET scanner:

1. Use NaI(Tl) as the detector material.
2. Focus our efforts on a small diameter system.
3. Image exclusively in three dimensions without septa.

The decision to use NaI(Tl) is largely based on the high light output of the scintillator. Anger-type position-sensitive NaI(Tl) detectors, using large photomultiplier tubes (PMTs), offer a cost-effective method of gamma-ray detection in nuclear medicine, and have been applied to 511-keV imaging since 1963 (*1*). Our group has designed several whole-body NaI(Tl) PET scanners (*2–4*), all based on hexagonal rings of six position-sensitive NaI(Tl) detectors, and most recently these same principles have been applied to a dual-detector SPECT/PET system (*5*). For this application to a dedicated brain-imaging scanner, we use a single annular crystal. For brain imaging, spatial resolution is often the most important consideration, particularly with positron-emitting isotopes with a short annihilation range, such as ^{18}F and ^{11}C. The single continuous detector leads to uniformly high spatial resolution, with fine spatial sampling, over the active area of the crystal, thus, high resolution in all three dimensions in the reconstructed images. A single continuous detector also avoids the need for scanner motion or compensation for missing data that result from having gaps between each pair of adjacent detectors used in the whole-body PENN-PET scanners (*3*).

A drawback with a continuous detector of NaI(Tl), which has

Received Mar. 22, 1996; revision accepted Jul. 22, 1996.

For correspondence or reprints contact: Joel S. Karp, PhD, Dept. of Radiology, Nuclear Medicine Section, Donner Rm. 110, University of Pennsylvania, 3400 Spruce St., Philadelphia, PA 19104.